

Science

Pancam and Microscopic Imager observations of dust on the Spirit Rover: Cleaning events, spectral properties, and aggregates

Alicia F. Vaughan¹, Jeffrey R. Johnson¹, Kenneth E. Herkenhoff¹, Robert Sullivan², Geoffrey A. Landis³, Walter Goetz⁴ and Morten B. Madsen⁵

¹U.S. Geological Survey, Flagstaff, AZ 86001, USA, afvaughan@usgs.gov; ²Center for Radiophysics and Space Research, Department of Astronomy, Cornell University, Ithaca, NY 14853, USA; ³NASA John Glenn Research Center, Cleveland, OH, 44135, USA; ⁴Max-Planck-Institut für Sonnensystemforschung, Katlenburg-Lindau, Germany; ⁵Niels Bohr Institute, University of Copenhagen, Copenhagen, Denmark

Citation: Mars 5, 129-145, 2010; doi:10.1555/mars.2010.0005

History: Submitted: March 15, 2010; Reviewed: May 20, 2010; Revised: August 2, 2010; Accepted: August 5, 2010; Published: December 10, 2010

Editor: Robert M. Haberle, NASA AMES Research Center

Reviewers: Nathan T. Bridges, Applied Physics Laboratory, Johns Hopkins University; William H. Farrand, Space Science Institute; Lori K. Fenton, Carl Sagan Center, SETI Institute

Open Access: Copyright © 2010 Vaughan et al. This is an open-access paper distributed under the terms of a [Creative Commons Attribution License](#), which permits unrestricted use, distribution, and reproduction in any medium, provided the original work is properly cited.

Abstract

Approach: The Mars Exploration Rover Spirit has experienced over 2000 martian days (sols) of interaction with the martian dust cycle. Much dust accumulated on the vehicle, but there have also been three major "cleaning events" when significant amounts of dust were removed. Pancam dust monitoring observations acquired every ~10 sols throughout the mission allowed visual inspection of the amount of dust collecting on a portion of the solar array and on the Pancam and Mini-TES calibration targets. Pancam multispectral data reveal three classes of airborne dust adhering to the capture and filter magnets: 1) "bright" capture magnet dust 2) "dark" capture magnet dust, and 3) filter magnet dust. Microscopic Imager (MI) images of the capture and filter magnets and a portion of the solar array aid in interpretation of behavior and morphology of the dust deposits.

Results: Three significant periods of "cleaning events" removed substantial amounts of dust from the rover. Each event occurred during southern hemisphere early spring and summer, and occurred later in the season of each successive Martian year. Pancam multispectral data of "bright" capture magnet dust exhibit the highest reflectance levels of the three classes. These spectra are also characterized by steep visible spectral slopes (434 to 673 nm), strong 535 nm absorptions, and are relatively featureless and convex in shape in the NIR region. "Dark" capture magnet dust has the lowest reflectance levels of the three classes, much shallower visible slopes and are much less "red" than the bright capture dust. They also have shallower 535 nm absorptions and are featureless in the NIR. They exhibit positive slopes from 900 to 1000 nm. Filter magnet dust shares spectral characteristics with the "dark" capture magnet dust, and together they represent a darker, more strongly magnetic component. Both Pancam and MI images reveal that the dust particles on the rover body cohere and form larger aggregates, measured at 100 μm to several mm. MI images of the rover magnets and body show that grains collected range from assumed (unresolved) dust size (< 4 μm) to fine sand (250 μm), and show that sand can saltate to a rover deck height of 70 cm in strong winds. Through comparisons with other data sets and previous work, we think wind speeds exceeding 20 m/s are responsible for the removal of dust during the cleaning events.

Implications: The spectral characteristics of the "bright" capture dust described here are consistent with multispectral observations of dust and bright soil elsewhere on the martian surface and support the theory that martian dust is globally mixed and deposited. This expanded data set also provides further evidence that the dust has a darker, more strongly magnetic component than typical bright dust. The large size of observed dust aggregates ($\geq 100 \mu\text{m}$) should make them easier to entrain by wind than individual dust grains, and therefore represent another process by which dust is lifted into the atmosphere. Entrainment of larger dust aggregates may represent a significant source of atmospheric dust loading wherever saltating sand is uncommon.

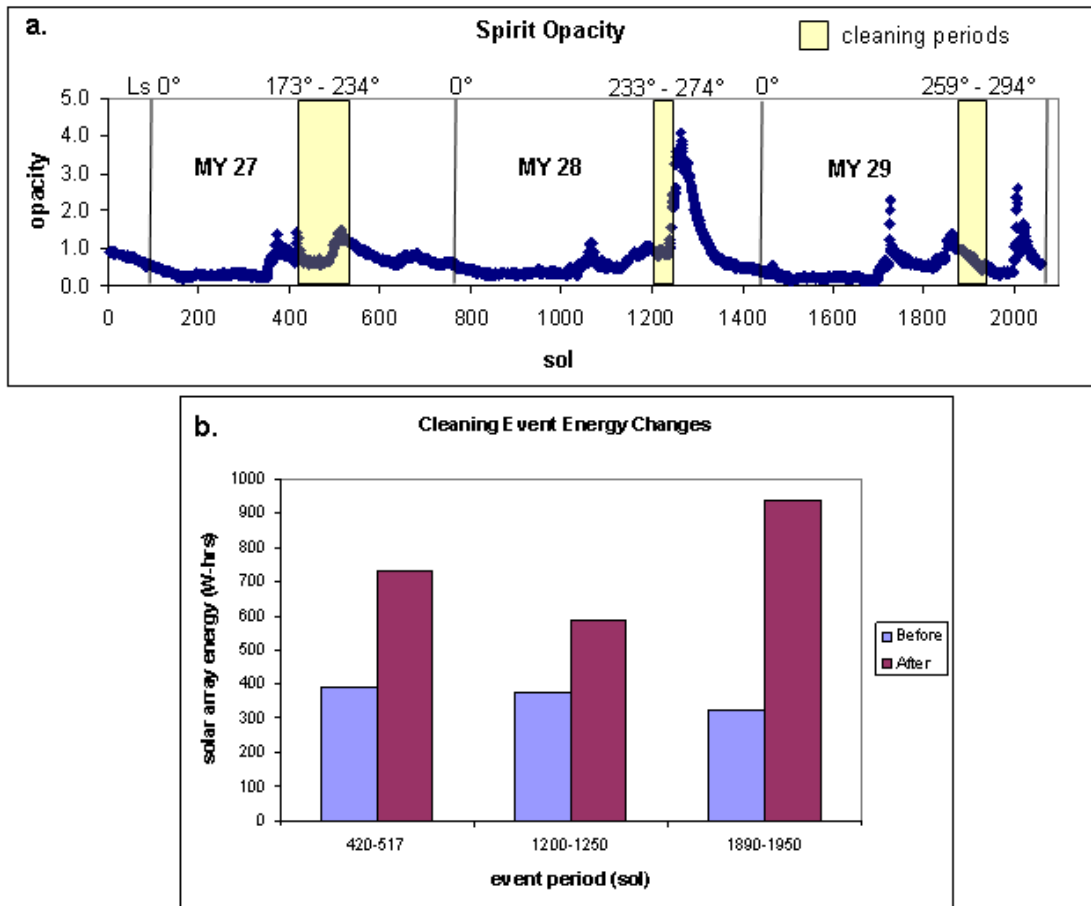


Figure 1. The three main periods of “cleaning events” Spirit experienced to date. **(a)** Atmospheric opacity by sol with the cleaning event periods highlighted in yellow and their respective L_s values labeled above. Vertical lines denote $L_s = 0^\circ$. The spike in opacity around Sol 1250 corresponds to the 2007 global dust storm. Opacity data are available online through the PDS ([figure1a.jpg](#)). **(b)** Changes in solar array energy during the three cleaning events ([figure1b.jpg](#)).

Introduction

Throughout the six years of exploration by the Spirit rover, the Athena suite of instruments has examined many aspects of dust at the Gusev landing site including composition ([Bell et al. 2004](#); [Goetz et al. 2005](#); [Yen et al. 2005](#); [Gellert et al. 2004](#); [Morris et al. 2004](#)), morphology and behavior ([Sullivan et al. 2008](#)), and magnetic components ([Madsen et al. 2009](#)). Here we describe results from observations made by the Panoramic Camera (Pancam) ([Bell et al. 2003](#)) and Microscopic Imager (MI) ([Herkenhoff et al. 2003](#)) of dust accumulation, removal, spectral characteristics, and morphology on the rover body. This data set provides insight into the composition of dust, the seasonality of significant wind events, and the aggregating nature of dust particles. The tendency of dust particles to form larger aggregates has implications for dust entrainment processes that might be useful for guiding numerical models of the martian atmosphere.

The solar arrays on Spirit are subject to continuous accumulation of airfall dust, but also to occasional wind-

related dust removal, or “cleaning events.” There have been three major cleaning events to date, all occurring in late southern winter ($L_s \sim 170$) to early summer ($L_s \sim 290$), but later in the season each successive Martian year (Figure 1). Cleaning events are recognized by an increase in power produced by the solar arrays ([Landis 2005](#)). The first significant cleaning event happened between Sols 417 and 520, characterized by a large event between Sols 417 and 420 ($L_s = 173$) that removed a substantial amount of dust from the vehicle and surrounding local terrain ([Johnson et al. 2006](#)), and greatly increased the solar power. Another significant event occurred on sol 519 ($L_s = 234$) removing more dust. Although the first of these events occurred during the same time period as the earliest appearances of dust devils observed by Spirit ([Greeley et al. 2006](#)), the event has been interpreted as very strong regional wind rather than a dust devil because regional albedo patterns revealed by MOC images across the Columbia Hills also changed during this time ([Sullivan et al. 2008](#)).

Subsequent cleaning events occurred between Sols 1187 ($L_s = 233$) and 1250 ($L_s = 274$), just before the onset of the 2007

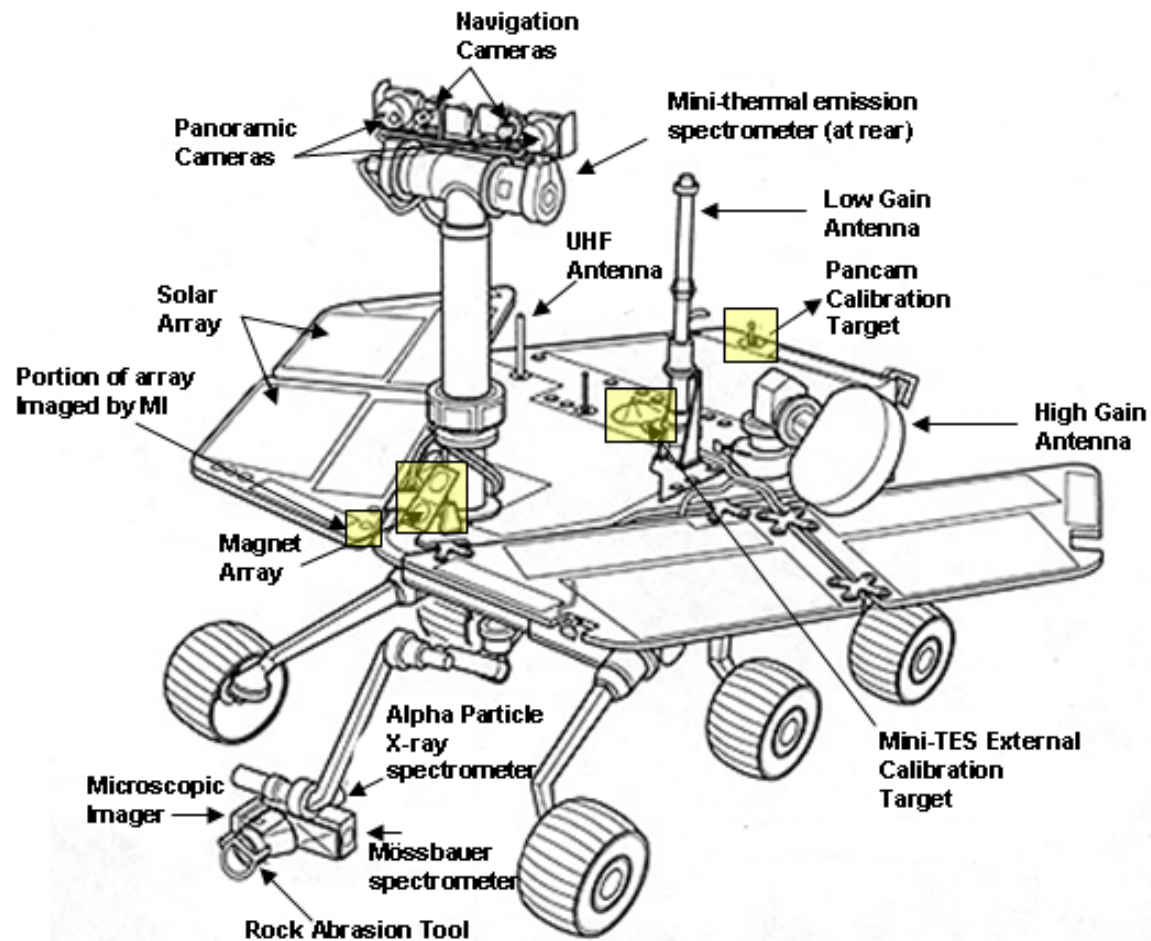


Figure 2. Rover diagram identifying key components of the vehicle. Areas highlighted in yellow boxes are places on the rover body imaged by Pancam and/or MI to monitor dust accumulation ([figure2.jpg](#)).

dust storm. The following Martian year, a major cleaning event began on Sol 1896 ($L_s = 259$), and smaller cleaning events continued up to about Sol 1950 ($L_s = 294$). This most recent event has been of particular importance to the mission as it increased the solar power by nearly a factor of 3 and lifted several power-related constraints on the strategic plan for the rover's attempted extrication from entrapment in fine-grained deposits at the location "Troy."

Grain size for those dust particles suspended in the atmosphere above Gusev has been retrieved from opacity measurements made by Pancam from the surface, and [Lemmon et al. \(2004\)](#) calculate this size to be $< 4 \mu\text{m}$ in diameter. Thus, this is likely the lower limit on grain size of dust that accumulates on the rover body. Some airfall particles could be a bit larger as they will settle out of the atmosphere more easily than the $4 \mu\text{m}$ dust particles in suspension. Larger sand size grains ($150\text{-}250 \mu\text{m}$) present on the rover body are assumed to have been emplaced by saltation.

Spectral characteristics of dust on the magnets through Sol 425 show that dust adhering to the filter magnet has a lower albedo (is darker) than dust adhering to the capture magnet

([Bertelsen et al. 2004](#); [Madsen et al. 2009](#)). [Madsen et al. \(2009\)](#) reported that "bright" and "dark" dust deposits are magnetically separated on the capture magnet, and suggested that dust layer thickness controlled the overall shape in the NIR portion of dust spectra. Specifically, they observed that thicker dust layers have maximum reflectance values from $750\text{-}950 \text{ nm}$ wavelengths, while thin dust layers commonly have reflectance minima in this region.

[Sullivan et al. \(2008\)](#) identified dust aggregates in local deposits investigated by the Spirit Rover. They were observed in soil deposits, as well as on rock surfaces and were demonstrated to be sufficiently fragile that they disintegrated upon contact with the Mössbauer contact plate at very low compression forces. [Sullivan et al. \(2008\)](#) hypothesized that these larger dust aggregates should be easier to entrain by wind than individual dust grains and could represent a significant source of atmospheric dust loads.

The work presented here expands on these previous studies to describe multispectral data and grain morphologies of dust deposits on the rover body through Pancam and MI observations of the magnets and solar array through Sol 2017

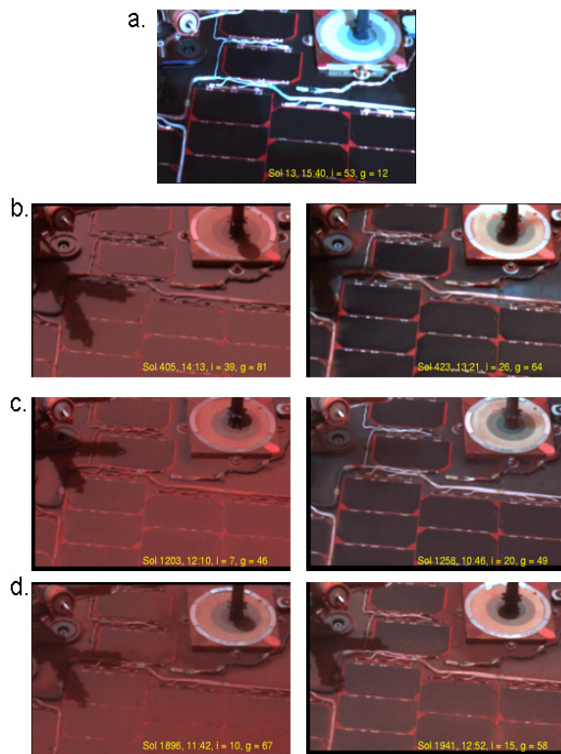


Figure 3. Pancam false color images of the Pancam calibration target and surrounding solar array cells. All images have been converted to R^* and stretched identically. The yellow text on each image denotes the sol number, local true solar time of image acquisition, incidence angle, i , and phase angle, g . (a) Image taken on Sol 013 of a clean rover. (b) Images taken on Sols 405 and 423 to illustrate the effects of the 417 - 420 cleaning event. (c) Images taken on Sols 1203 and 1258 illustrating the cleaning events between Sols 1200 and 1250. (d) Images taken on Sols 1896 and 1941 illustrating the latest cleaning events that occurred between Sols 1890 and 1950 ([figure3.jpg](#)).

of the Spirit mission.

Pancam dust observations

Dust monitoring

The Pancam consists of two 1024×1024 CCD cameras mounted approximately 1.5 m above the ground that are capable of stereoscopic, multispectral observations ([Bell et al. 2003](#)). Pancam can collect data in 16 filters or wavelength bands, 13 of which are used as the distinct “geology” filters for multispectral observations. Pancam used a standardized observing sequence to image the Miniature Thermal Emission Spectrometer (Mini-TES) and Pancam calibration targets and the surrounding solar array cells that help monitor currents and voltages every ~10 sols throughout the mission (Figure 2). This image sequence uses 2×2 downsampled, L2, L6, and L7 filters (753 nm, 482 nm, and 432 nm, respectively). Figure 3 shows before and after image pairs of the Pancam calibration target bracketing the three main cleaning events of the mission thus far.

Using data from the calibration target and pre-launch calibration information, raw Pancam images were calibrated to radiance and then to radiance factor I/F (where I is the measured radiance and πF is the incident solar irradiance). The solar incidence angle recorded for each scene was used to convert the I/F data to relative reflectance (R^* , defined as I/F divided by the cosine of the incidence angle ([Reid et al. 1999](#)). [Bell et al. \(2006\)](#) estimated the absolute reflectance levels of these data to be accurate to within ~10% at the shortest wavelengths, and slightly more accurate at longer wavelengths. Relative filter-to-filter uncertainties in R^* were estimated to be typically 1-5%.

After a significant amount of dust has accumulated on the deck, the dust particles start to cohere forming much larger dust aggregates. This is evident through visual inspection of the Pancam images of the rover deck surrounding the Mini-TES calibration target, an example of which is shown in Figure 4. The aggregating behavior of dust particles will be discussed in more detail in later sections.

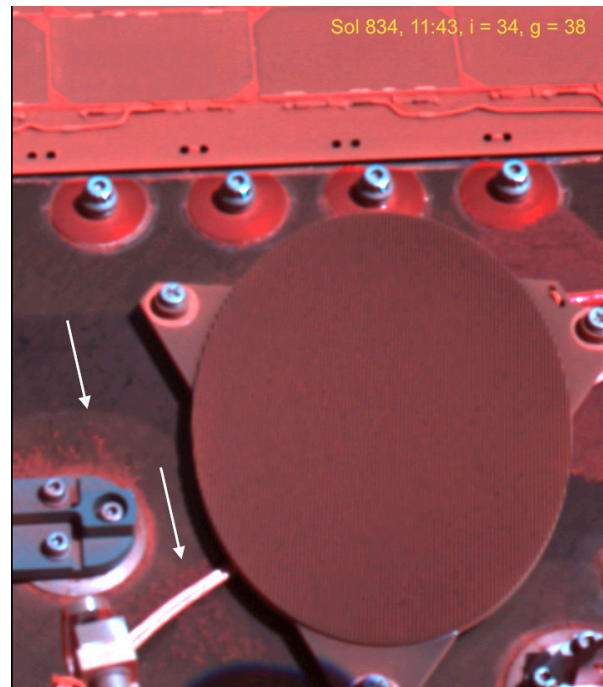


Figure 4. Pancam false color image of Mini-TES calibration target showing the clumping nature of the dust particles that collect on the rover body. The yellow text embedded in the image denotes sol number, local true solar time, incidence, i , and phase angle, g , for the image. The arrows call out areas where the dust particles cohere to form larger aggregates ([figure4.jpg](#)).

Multispectral data of magnet dust

The capture and filter magnets are mounted on the rover deck in front of the mast and are inclined at a 45° angle from the rover deck surface in order to collect airfall dust and be reachable for analysis by the instruments on the robotic arm (Figure 2). The magnet component is made of $\text{Sm}_2\text{Co}_{17}$, and is embedded in an aluminum structure and covered by an

Table 1. Pancam magnet observations viewing geometry details.

Sol	Sequence ID	Local True Solar Time	*Incidence	**Emission	Phase
184	p2149	11:02:37	38.6	-4.1	42.7
307	p2113	12:09:49	37.6	-11.9	31.9
425	p2113	14:49:13	45.1	-16.6	33.2
545	p2113	12:44:41	13.8	-10.0	13.1
954	p2113	12:06:40	39.1	-11.2	28.1
1351	p2113	10:56:58	15.9	-4.2	17.8
1846	p2113	13:42:49	24.9	-3.4	21.6
2091	p2113	11:14:41	22.8	-16.6	37.0
2102	p2113	11:56:27	22.1	-16.9	32.2
2102	p2113	16:16:28	67.3	-16.9	53.6

*Incidence angle is defined in SITE coordinates relative to a horizontal surface.

**Emission angle is defined in SITE coordinates here, with -90 equivalent to the horizon.

aluminum foil (Madsen et al. 2003). The circular magnet structures have a 45 mm diameter. The capture is the stronger of the two magnets and was designed to collect most magnetic particles from the airborne dust, whereas the filter magnet is weaker and is designed to catch only the very strongly magnetic particles from the airborne dust (Madsen et al. 2003).

Semi-regular Pancam observations were made of the capture and filter magnets using the 13 “geology” filters (13-filter) spanning the spectral range 434 nm to 1009 nm, allowing for multispectral analysis of dust deposits on the magnets. The data set used here is comprised of Pancam 13-filter data collected on the magnets from Sols 184, 307, 425, 545, 954, 1351, 1846, 2091, and 2102. On Sol 2102 the observation was repeated at a different time of day in order to examine spectral differences caused by varying lighting geometry. Table 1 lists these observations along with their sequence identification number, local true solar time the observation was acquired, and incidence, emission, and phase angles describing the viewing geometry.

Multispectral analysis

For each of these observations, Pancam R^* of dust on the capture magnet and dust on the filter magnet were extracted and analyzed. Spectra of the non-magnetic (aluminum) border regions of the magnets have been collected in most cases in order to characterize the “background.” Whenever there were both “bright” and “dark” dust deposits on the capture magnet, spectra of both populations were extracted (Sols 425, 545, 1351, 1846, 2091, and 2102). The Pancam color composite images for each observation showing defined regions of interest corresponding to the spectra are shown in Figure 5, with the exception of Sol 2102 which is shown in Figure 7. The illumination azimuth can be inferred from looking at the shadow positions in the images. The Sol 307 image shows a soil clod on the filter magnet that was picked up from the surface and deposited by the contact plate of the Mössbauer spectrometer on the robotic arm when it was scheduled for integration on the filter magnet. The soil clod is absent in the Sol 425 image, presumably because it has fallen off the surface of the magnet during motion of the rover. Disturbances left in the dust layer were subsequently

removed during the Sol 417 - 420 cleaning event.

The border regions of the magnet structures that have no underlying magnet ($\text{Sm}_2\text{Co}_{17}$) are relatively dust free, although some dust does accumulate in and around micron(s) deep holes caused by sandblasting the surface during fabrication, and after long periods of dust accumulation. Spectra of these relatively dust-free border regions on the magnets’ aluminum surface are characterized by very shallow visible slopes, and broad 800 nm absorptions resulting in a concave shape for the near infrared (NIR) region from 700 nm to 1000 nm (Figure 6, Supplemental Figure 1). These characteristics define a background spectrum for purposes of discussion here. Spectra for three classes of dust: 1) “bright” capture magnet dust 2) “dark” capture magnet dust, and 3) filter magnet dust will be described below. There were no statistically meaningful changes in the spectra of the three dust classes over the span of the mission thus far, and so simple averages were computed for each class and shown in Figure 6. Supplemental Figure 1 shows color-coded spectra corresponding to each region of interest shown in Figure 5 for each sol including standard deviations, except for the Sol 2102 data, which are shown in Figure 7.

The bright dust adhering to the capture magnet has the highest reflectance of the three classes, with spectra characterized by steep visible slopes from 432 nm to 673 nm as well as very strong 535 nm absorptions (Figure 6 and Supplemental Figure 2). Bright dust spectra have an overall convex shape in the NIR (700 nm to 1000 nm), and are relatively featureless in that region. While Figure 6 shows an average spectrum for bright dust, it should be noted that the spectrum for the soil clod deposited on the filter magnet from Sol 307 is consistent with the bright dust adhering to the capture magnet (Supplemental Figure 1). This similarity suggests that the top layer of soil is likely airfall dust, as discussed by Madsen et al. (2009). The Sol 425 spectrum mostly resembles the background and is consistent with a relatively thin coating of dust following the Sol 417 - 420 cleaning event. Therefore, the bright dust spectrum for this sol was left out when computing the average spectrum for bright dust on the capture magnet.

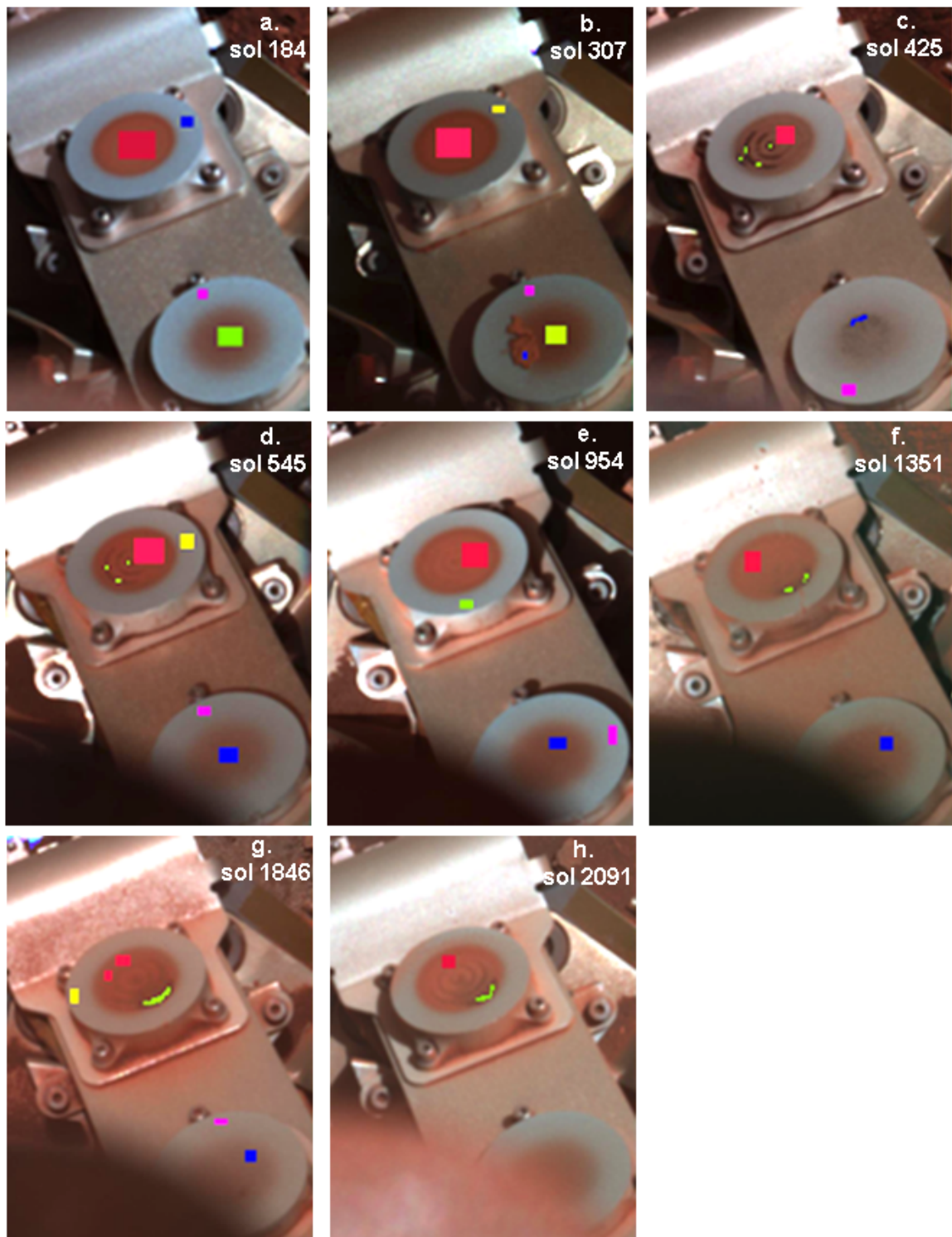


Figure 5. Pancam false color composite images (L2 = 753 nm, L5 = 535 nm, L6 = 482 nm) of the capture and filter magnets with designated regions of interest defining where spectra were taken (Supplemental Figure 1). In these images the capture magnet is at the top and the filter magnet is on the bottom. The sol number for each observation is in the upper right corner of the image. Blurry region at lower left is deployed lens cap. ([figure5a.jpg](#), [figure5b.jpg](#), [figure5c.jpg](#), [figure5d.jpg](#), [figure5e.jpg](#), [figure5f.jpg](#), [figure5g.jpg](#), [figure5h.jpg](#))

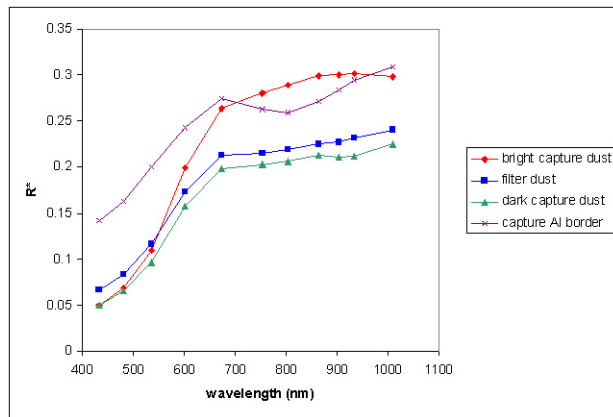


Figure 6. Computed average spectra for the three classes “bright” capture magnet dust, “dark” capture magnet dust, and filter magnet dust. Also shown is the average spectrum for the aluminum border region of the capture magnet ([figure6.jpg](#), [figure6.txt](#)).

The “bright” and “dark” dust deposits on the capture magnet appear as distinct populations after wind events, (see Figure 5, Sol 425). The “dark” dust on the capture magnet has the lowest reflectance levels of the three classes, with relatively shallow visible slopes, and is much less bright at 673 nm (less red). The “dark” capture magnet dust also has shallower 535 nm absorptions (Figure 6, Supplemental Figure 2). There are no meaningful features in the NIR region (700-1000 nm), and it lacks the overall convex shape shown in this region by the “bright” capture magnet dust. In fact, it is characterized by a positive slope from 900 nm to 1000 nm (Supplemental Figure 3).

In general, less dust adheres to the filter magnet, which was expected given its design and purpose ([Madsen et al. 2003](#)). The filter magnet spectral data set is also smaller because the left eye Pancam images become more obscured due to the rover’s pitch later in the mission by the lens cap that came off prior to first use of the camera and hangs down by a tether. In later sols, the cap is encroaching on the area over the filter magnet (see Figure 5, Sol 2091 and Figure 7 Sol 2102 images), and a reliable spectrum cannot be retrieved. The filter magnet dust is spectrally similar to the “dark” capture magnet dust with low relative reflectance, much shallower visible slopes, and is less “red” than the bright capture magnet dust (Figure 6). The filter magnet dust spectra also have shallower 535 nm band depths (Supplemental Figure 2), and are relatively featureless in the NIR (700-1000 nm) region. Filter dust spectra also lack the convex shape in the NIR region shown by the brighter dust on the capture magnet. Like the sol 425 bright capture magnet dust spectrum, the Sol 425 filter magnet dust spectrum resembles the background due to the Sol 417 - 420 cleaning event and has been left out of the calculation for average filter dust shown in Figure 6.

On Sol 2102, Pancam 13-filter magnet observations were taken at 11:56 LTST (2102am) and 16:16 LTST (2102pm) in order to determine if changes in viewing geometry altered the spectral features of dust on the magnets. The Sol 2102pm

spectra have higher reflectance and a greater positive slope from 673 nm to 1009 nm (Figure 7). While this may result from photometric properties of the dust accentuated by the higher incidence and phase angles of the 2102pm observations, we note that the magnet images were calibrated to R^* without accounting for their 45° inclination. Over the viewing angles considered here, the dominant effect of calibrating images of an inclined surface using a flat calibration target is to make the afternoon (2102pm) spectra brighter in the red wavelengths than the sol 2102am spectra owing to the nature of the martian atmosphere, which scatters more in the red wavelengths at higher incidence angles (e.g., [Johnson et al. 2006](#)). Despite the greater positive NIR slope observed in the sol 2102pm spectra, the spectral characteristics described for both “bright” and “dark” capture magnet dust remain. Their relative reflectance levels, 535 nm absorptions, spectral shape and absence of NIR features are not affected. This experiment suggests that varying the lighting geometry over phase angles of 13-54° has little to no effect on the characteristic spectral features described for each of the dust classes described here.

Microscopic Imager dust observations

The Microscopic Imager (MI) is one of the four instruments located on the end of Spirit’s robotic arm. It is a 1024×1024 CCD camera with a best-focus resolution of 31 μm per pixel and simulates a geologist’s hand lens in terms of resolution ([Herkenhoff et al. 2003](#)). The robotic arm allows the MI to approach the magnets and a portion of the solar array for imaging. Martian atmospheric dust particles are < 4 μm in diameter ([Lemmon et al. 2004](#)), well below the resolution of the MI. However, the MI can resolve fine sand-sized grains as small as about 100 μm . All particle sizes reported in this work were measured by counting pixels across the diameter, and using the best focus MI resolution of 31 $\mu\text{m}/\text{pixel}$. Although the MI is not used as frequently as the Pancam for dust monitoring, the images are very helpful for understanding the dynamic nature and morphology of the dust particles.

MI images of the capture magnet

As described earlier, the capture magnet is stronger than the filter magnet. The $\text{Sm}_2\text{Co}_{17}$ component of the capture magnet consists of a central cylinder surrounded by three concentric rings with an overall diameter of 25 mm embedded within an aluminum structure ([Madsen et al. 2003](#)). Seven MI images of the capture magnet were selected for analysis because they have good illumination and were obtained close in time to when Pancam 13-filter data were acquired. These MI images from sols 240, 505, 1006, 1230, 1355, 1504, and 2017 illustrate cleaning events, the presence of both “bright” and “dark” dust deposits, and the aggregating nature of dust particles.

The Sol 240 MI image shows a significant dust coating on the capture magnet, along with an aggregate of dust ~400 μm across (Figure 8a). The individual grains comprising the aggregate cannot be resolved and are assumed to be airfall

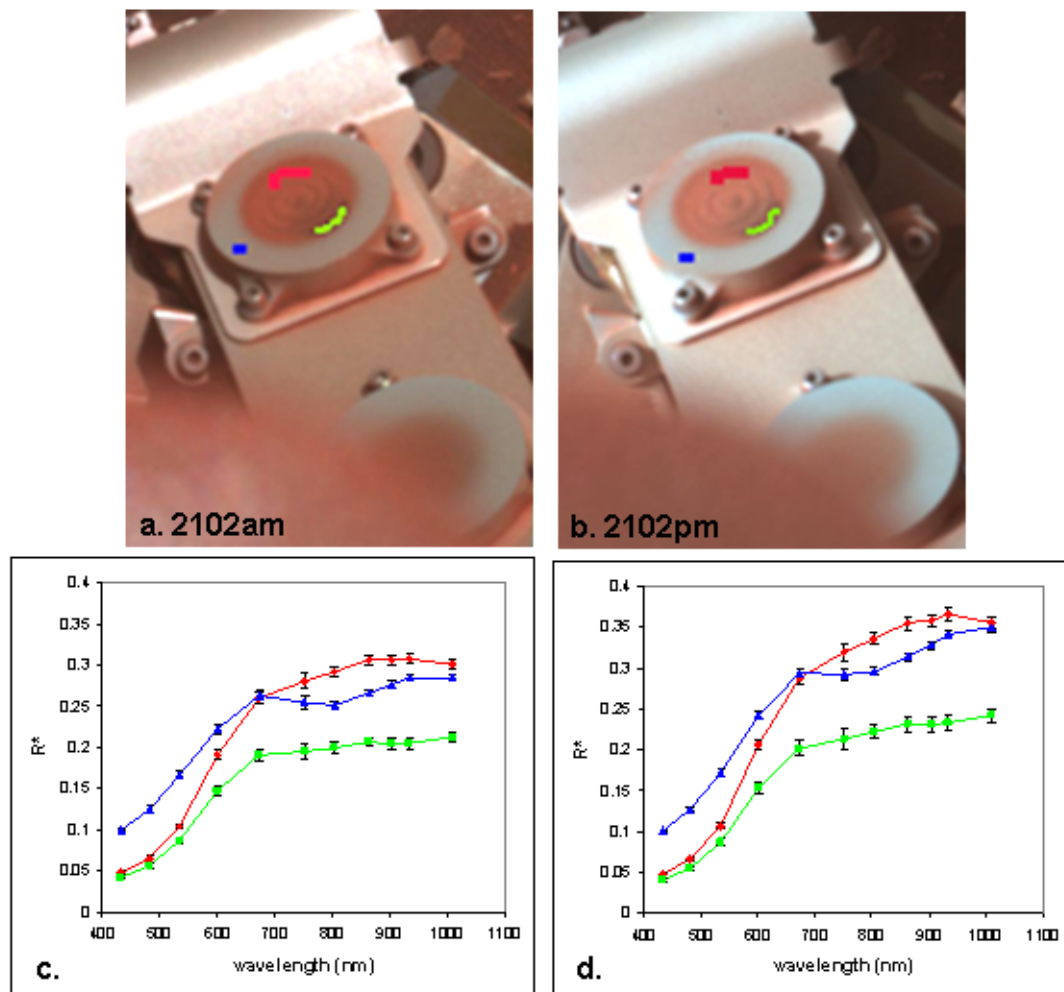


Figure 7. Sol 2102 13-filter magnet data showing the Pancam false color composite images (L2 = 753 nm, L5 = 535 nm, L6 = 482 nm) for both **(a)** 11:56 LTST (2102am) ([figure7a.jpg](#)) and **(b)** 16:16 LTST (2102pm) ([figure7b.jpg](#)) with the defined regions of interest ([figure7b.jpg](#)). **(c)** shows the color-coded spectra ([figure7c.txt](#)) representing the regions of interest in (a), and **(d)** shows the spectra representing the regions of interest in (b). The capture magnet is at the top of the images and the filter magnet is on the bottom. Note the obstruction of the filter magnet by the lens cap prohibiting the collection of filter dust spectra ([figure7d.txt](#)).

dust grains. Alternatively, the 400- μm particle could be a solid sand grain that has saltated up from the surface. However, ~150-250 μm sand grains lack concave-out grain boundary segments (see Figure 10b). Also, this grain is much larger than the most easily saltated grain size for Mars which is 100-150 μm ([Greeley et al. 1980](#); [Iversen and White 1982](#)). No substantial wind events had been noted at this point in the mission that could explain the saltation of larger sand particles, particularly to the height of the magnets.

The image from Sol 505 (Figure 8b) shows the effects of the Sol 417-420 cleaning event. Much of the fine-grained material has been removed and a population of strongly magnetic, $\leq 100 \mu\text{m}$ dark grains has been left aligned above the space in between the underlying magnetic rings. This behavior is caused by the strong magnetic field gradients between the adjacent magnetic rings of opposite polarity. [Merrison et al. \(2002\)](#) reported that in wind tunnel

experiments of magnetic capture of martian aerosols no significant dust removal occurs at wind speeds less than 20 m/s. These wind tunnel experiments were performed at martian atmospheric pressures, with Salten Skov soil as an analogue to martian dust. This naturally occurring soil is reported to be composed of over 60% by weight iron oxides including 13% maghemite, 14% hematite, with the rest assigned to goethite. The remaining 40% is composed of silicates, and all particles are $\sim 2 \mu\text{m}$ in diameter upon dispersion. On the basis of these analog experiments, the removal of dust from the Spirit magnets indicates that wind speeds exceeded 20 m/s at the $\sim 75 \text{ cm}$ height of the magnets during the Sol 417-420 cleaning event.

By Sol 1006 there had been considerable dust deposition and many large aggregates had formed, casting shadows in the MI image. The aggregates range from 200 to 400 μm across (Figure 8c). Based on the variety of particle shapes and sizes,

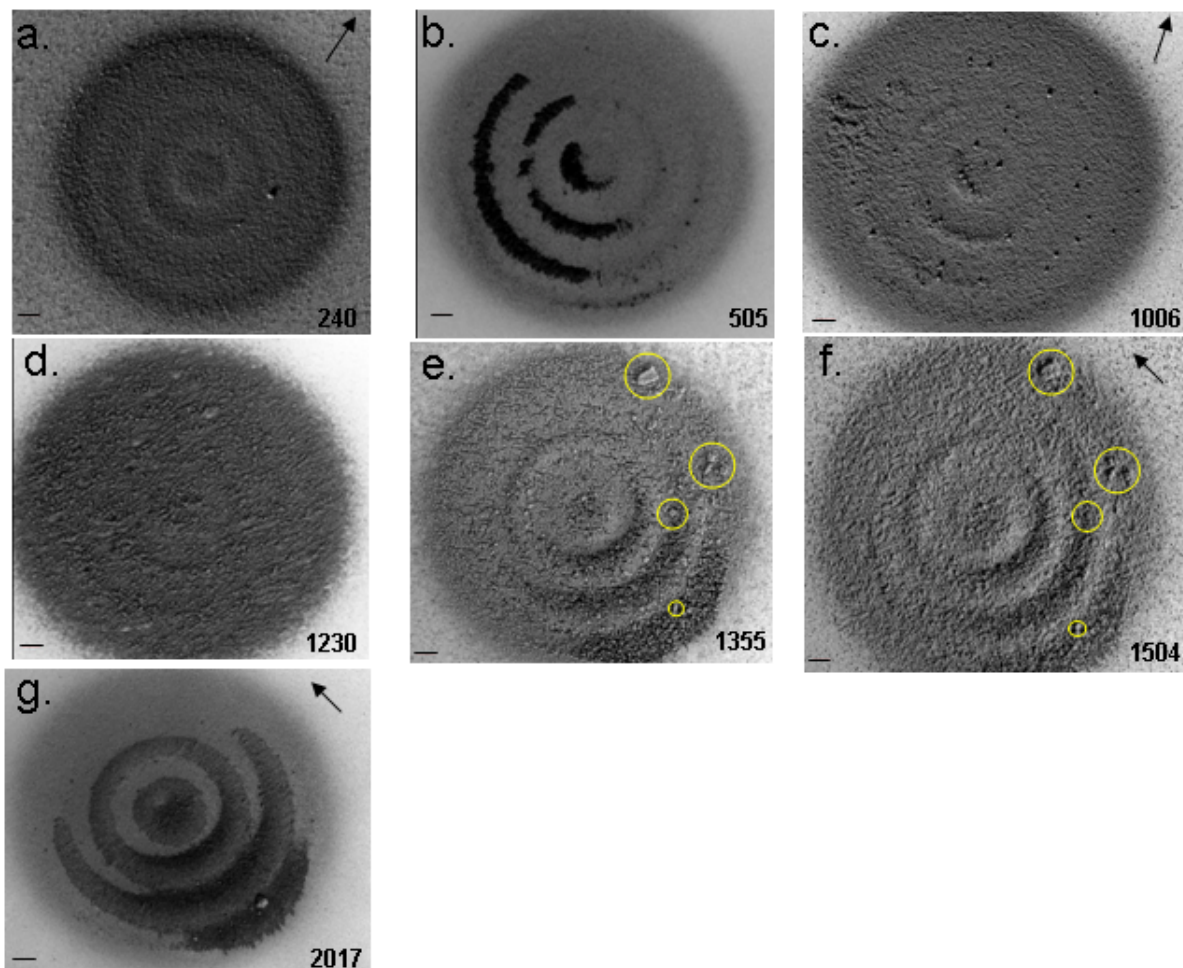


Figure 8. MI images of the capture magnet. Scale bar in each image represents 1.5 mm. Sol number is labeled in the lower right hand corner of each image. Yellow circles in (e) and (f) call out grains that were stationary between sols 1355 and 1504. Arrows in the upper right corner of the images denote illumination direction, and those images without arrows were acquired in shadow. ([figure8a.jpg](#), [figure8b.jpg](#), [figure8c.jpg](#), [figure8d.jpg](#), [figure8e.jpg](#), [figure8f.jpg](#), [figure8g.jpg](#))

the lack of clear grain boundaries, and the large grain sizes (making saltating sand an unlikely origin for these particles in the absence of very strong winds), these particles are interpreted to be dust aggregates. In the Sol 1230 MI image, the bumpy or “fluffy” texture indicates that the dust is cohering to form larger aggregates (Figure 8d). Grain sizes are very difficult to measure on this image because grain boundaries are not easily identified. Long, narrow troughs criss-cross the dust deposit on the magnet. Troughs have widths and probably depths similar to typical aggregate diameters, but their lengths are many times greater. We interpret these features as texture imposed by wind effects (Sullivan et al. 2008). It is likely that the troughs formed when wind mobilized dust aggregates to roll along the magnet surface. Saltation impacts from hard sand grains seem less likely to be responsible, because such impacts probably would leave much shorter marks.

The Sol 1355 MI image shows mounds of dust aligned along the voids between the magnetic rings in the lower right portion of the image (Figure 8e), and close inspection reveals

brighter dust aggregates overlying dark dust deposits in these areas. Recall that the 2007 dust storm started around Sol 1250, and was likely responsible for some of the changes seen between images taken on Sols 1230 and 1355, including more dust deposition and the movement of the concentration of darker grains in the leftmost position of the sol 505 image (Figure 8b) towards the lower right portion of the magnet (Sol 1355). It is also possible that high winds during the dust storm completely removed the earlier population of dark grains, and that the dark grains seen in the lower right portion of the Sol 1355 image are new deposits. A significant thickening of the layer of more magnetic particles is seen between the Sol 1230 and the Sol 1355 images. There are small grain tracks in the Sol 1355 image, evidence for motion of the 150 μm to 300 μm dust aggregates. The large particle in the upper right portion of the image measures ~ 1.5 mm in diameter. It is difficult to determine by morphology alone whether this particle is an aggregate or a coarse sand grain with dust deposited on it. The grain boundaries can be resolved, and there was significant wind activity prior to this image being taken, making it possible that sand could have

saltated to the height of the magnets. However, this grain is significantly larger than the expected range of saltating grains for Mars. It is also possible that this is a soil or dust deposit shed off one of the instruments on the robotic arm as it approached the magnets for imaging. We prefer the interpretation that this is a dust aggregate.

The Sol 1504 image shows additional, thicker dust deposition without much disturbance, and although individual grains are not resolved, there is an evident texture that is apparently caused by the coherence of dust particles (Figure 8f). The mounds of dust aligned along the magnetic rings in the Sol 1355 image are still present as well as the large (~1.5 mm) aggregate in the top right portion of the image. The positions of many identifiable aggregates have not changed appreciably between Sols 1355 and 1504 attesting to the strong magnetic adherence force for these aggregates and the relative quiescence of the atmosphere (see circled grains in Figure 8e,f). Wind-related textures in the Sol 1355 image have been partly erased by dust deposition, and partly replaced with subtle wind-related textures along a different azimuth.

The capture magnet was not imaged again until Sol 2017, after the most recent cleaning event (Sols 1896-1950). Strikingly similar to the Sol 505 image except for the exact position of the deposits (post-420 cleaning event), much of the fine grained and brighter material has been removed leaving behind the darker, $\leq 100 \mu\text{m}$ strongly magnetic population of grains aligned along the voids between magnetic rings (Figure 8g). These grains represent the same material that formed the mounds seen in the Sol 1355 and 1504 images after the overlying “brighter” and less strongly magnetic dust aggregates have been removed. There are a few larger particles present, up to approximately $200 \mu\text{m}$, and one very coarse grain approximately 0.9 mm in diameter. This grain has distinct boundaries, and since the overlying, brighter dust aggregates were removed in the cleaning event, it is possible that this is a sand grain. Although it is very large to have saltated to the height of the magnets, this possibility cannot be ruled out. Again, it is also possible that this particle was dropped onto the magnet off of the robotic arm when it came up to magnets for imaging, however, there is no disturbance in the surrounding dust suggesting an impact, and with the magnets tilted at 45° , the particle is almost certainly magnetic or it would have fallen to the surface.

MI images of the filter magnet

As mentioned before, the filter magnet is designed to collect only the strongly magnetic particles of airborne dust, and thus much less dust adheres to this magnet. However, the MI images of the filter magnet presented here (Figure 9) illustrate the diversity of dust deposits. The $\text{Sm}_2\text{Co}_{17}$ component of the filter magnet is a modified ellipsoid with a base diameter of 25mm embedded within an aluminum structure (Madsen et al. 2003).

The image from Sol 240 shows a thin coating of dust collected on the filter magnet. The grains are $<150 \mu\text{m}$ in

diameter (Figure 9a). The Sol 963 MI image shows a scattering of $\leq 200 \mu\text{m}$ sand grains in the dust, some of which are casting shadows in the image (Figure 9b). The Sol 1128 image shows more dust accumulation, one larger aggregate measuring $\sim 250 \mu\text{m}$ across, and many smaller aggregates measuring $\leq 150 \mu\text{m}$ (Figure 9c). The large grain in the right half of the image measures $\sim 1 \text{ mm}$ on its long axis, and has a very different morphology from the surrounding dust aggregates. It is possible that this is a sand grain, although it seems unlikely that it could have saltated up to the filter magnet in the absence of any significant wind events since the last image of the filter magnet. It is possible that it is a clump of soil that dropped off of the robotic arm when it was positioned above the magnet for imaging. Note the subtle trace left as a result of movement of this particle towards the center of the magnet where the force of attraction is maximum.

The Sol 1239 image (Figure 9d), was taken prior to the 2007 dust storm, and clearly shows the erosive effects of high winds that preceded the main high opacity event related to the 2007 dust storm. The aggregates from previous sols had been altered or removed, leaving behind small, dark grains measuring $< 100 \mu\text{m}$. Horizontal wind tracks are also visible. By Sol 1358 (Figure 9e), the dust storm had subsided and the sky above Spirit was clearing (Figure 1). Much new dust had accumulated on the filter magnet including many brighter dust aggregates similar to those present on the capture magnet (Figures 9e and 8e). The largest aggregate in the image measures $\sim 350 \mu\text{m}$, but most are $\leq 150 \mu\text{m}$. In the bottom portion of the image the brighter dust aggregates are overlying darker, smaller grains, similar to the capture magnet deposits at this time. The Sol 1473 filter magnet image is not significantly different from the Sol 1358 image, other than that the aggregates are on average larger (Figure 9f). The largest aggregate in the image is $\sim 450 \mu\text{m}$ in diameter, while most are $\leq 200 \mu\text{m}$.

MI images of the solar array

A small section of the solar array can be viewed by the MI (Figure 2). MI images of the solar array have been acquired nine times during the mission thus far. Five images are presented here based on their quality of illumination and temporal proximity to MI images of the magnets (Figures 10 and 11).

The image from Sol 505 was acquired after the Sol 417 -420 cleaning event (Figure 10a). The diffuse reflectance of the array is a sign of dust deposition, as a clean array would appear more like specular glass (Landis et al. 2006). A population of well rounded, well sorted sand grains ranging from 150 to $250 \mu\text{m}$ in diameter have collected near some of the cables on the deck at a height of 70 cm from the ground (Figure 10a,b). Wind tunnel experiments show that the easiest grain size for wind to move on Mars is 100 - $150 \mu\text{m}$ (Greeley et al. 1980; Iversen and White 1982). However, saltation heights for these particles are not well known (White 1979; Greeley and Iversen 1985; Greeley et al. 1992). It appears on the basis of the MI images and the work of Merrison et al. (2002) that with very strong winds (>20

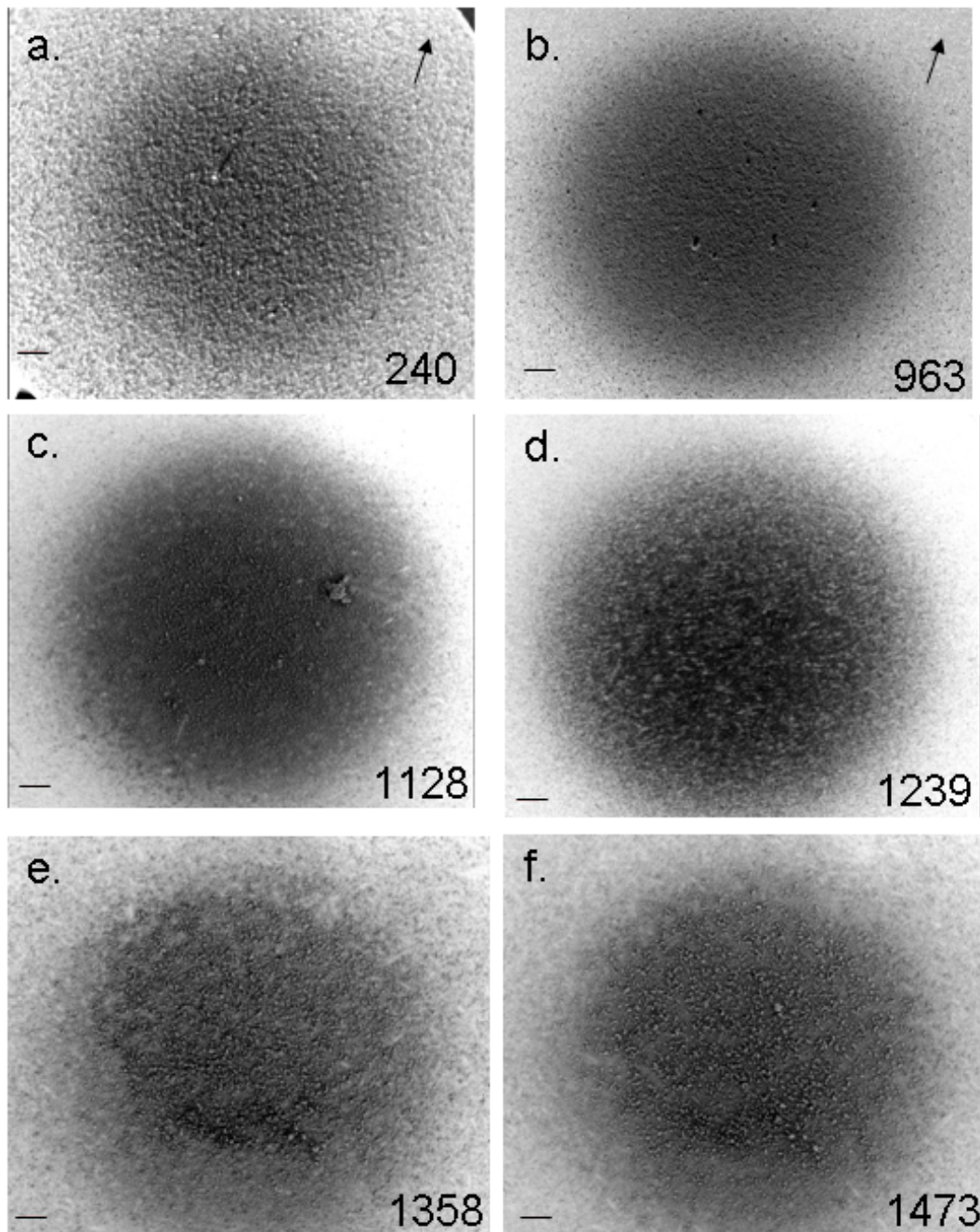


Figure 9. MI images of filter magnet. Scale bar in each image represents 1.5 mm. Sol number is labeled in the lower right hand corner. Arrows in the upper right corner of the images denote illumination direction, and those images without arrows were acquired in shadow. ([figure9a.jpg](#), [figure9b.jpg](#), [figure9c.jpg](#), [figure9d.jpg](#), [figure9e.jpg](#), [figure9f.jpg](#))

m/s), it is possible for sand grains to saltate to at least 70 cm, the height of the rover deck.

The sol 1006 MI image (Figure 10c) shows that fine-grained material had continued to collect in pockets around the cabling on the deck. However, the sand grains from Sol 505 are gone, having either been removed entirely or simply moved to another location on the deck. The Sol 1230 view shows increased dust deposition on the array as well as wind tracks (Figure 10d). The images from Sol 1473 show many

dust aggregates (Figure 11). Most aggregates are similar in size ($\leq 150 \mu\text{m}$) and appearance to those observed on the magnets (Figures 8 and 9). However, there are a few much larger aggregates, including an elongated aggregate that extends beyond the edge of the image. The visible portion is nearly 8 mm long and 1.5 mm wide. These larger aggregates have darker halos surrounding them where it looks as though surrounding dust grains have been removed from the array to help form them, suggesting that the aggregates (at least partly) formed in situ. It is possible that these larger

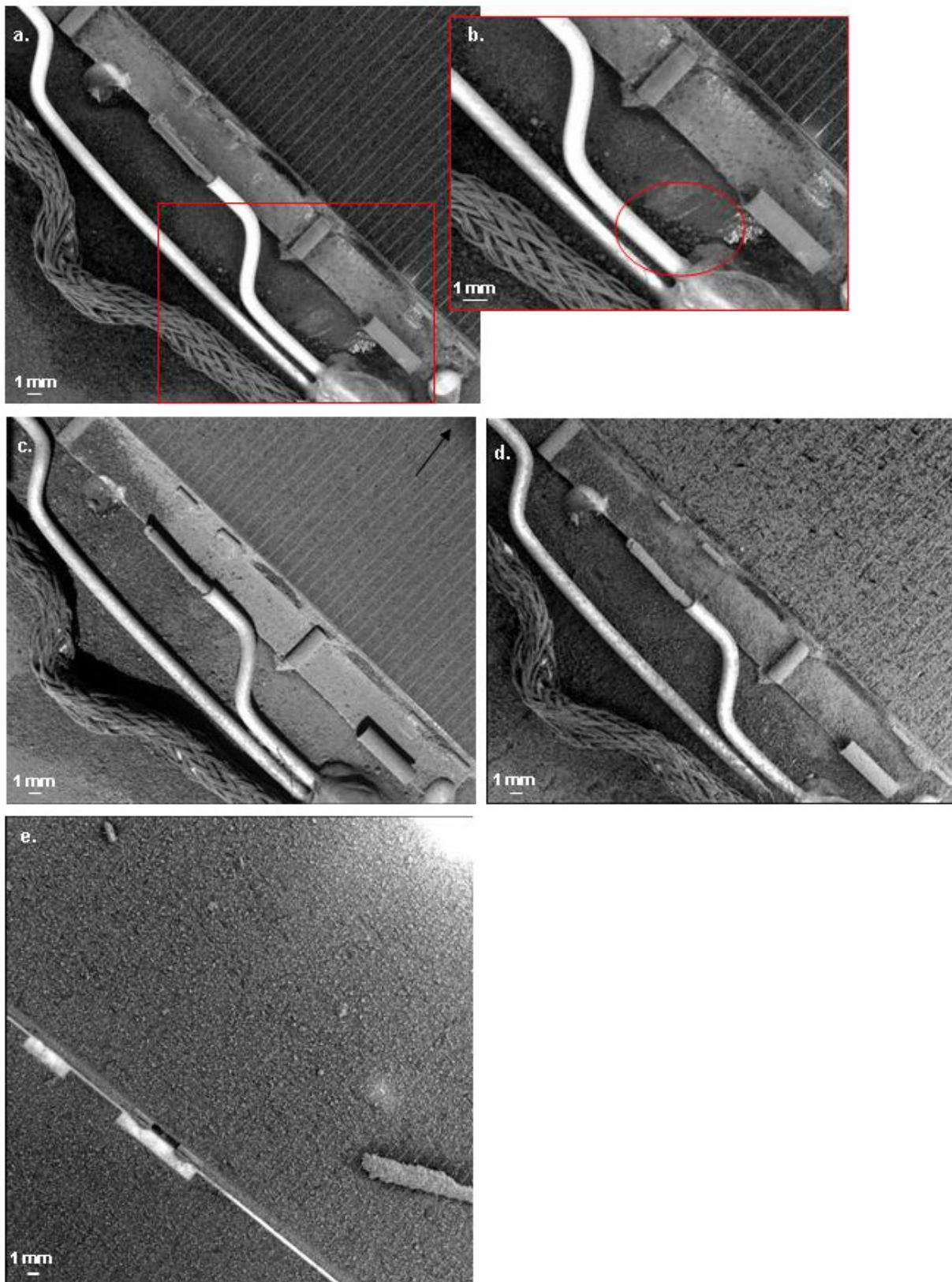


Figure 10. MI images of the solar array. **(a)** Image from Sol 505 ([figure10a.jpg](#)) with red box denoting area shown in **(b)** Zoom of Sol 505 image with red circle around 150 to 250 μm sand grains. **(c)** Image from Sol 1006 ([figure10c.jpg](#)). **(d)** Image from Sol 1230 ([figure10d.jpg](#)). **(e)** Image from Sol 1506 of adjacent section of array ([figure10e.jpg](#)). Arrows in the upper right corner of the images denote illumination direction, and those images without arrows were acquired in shadow.

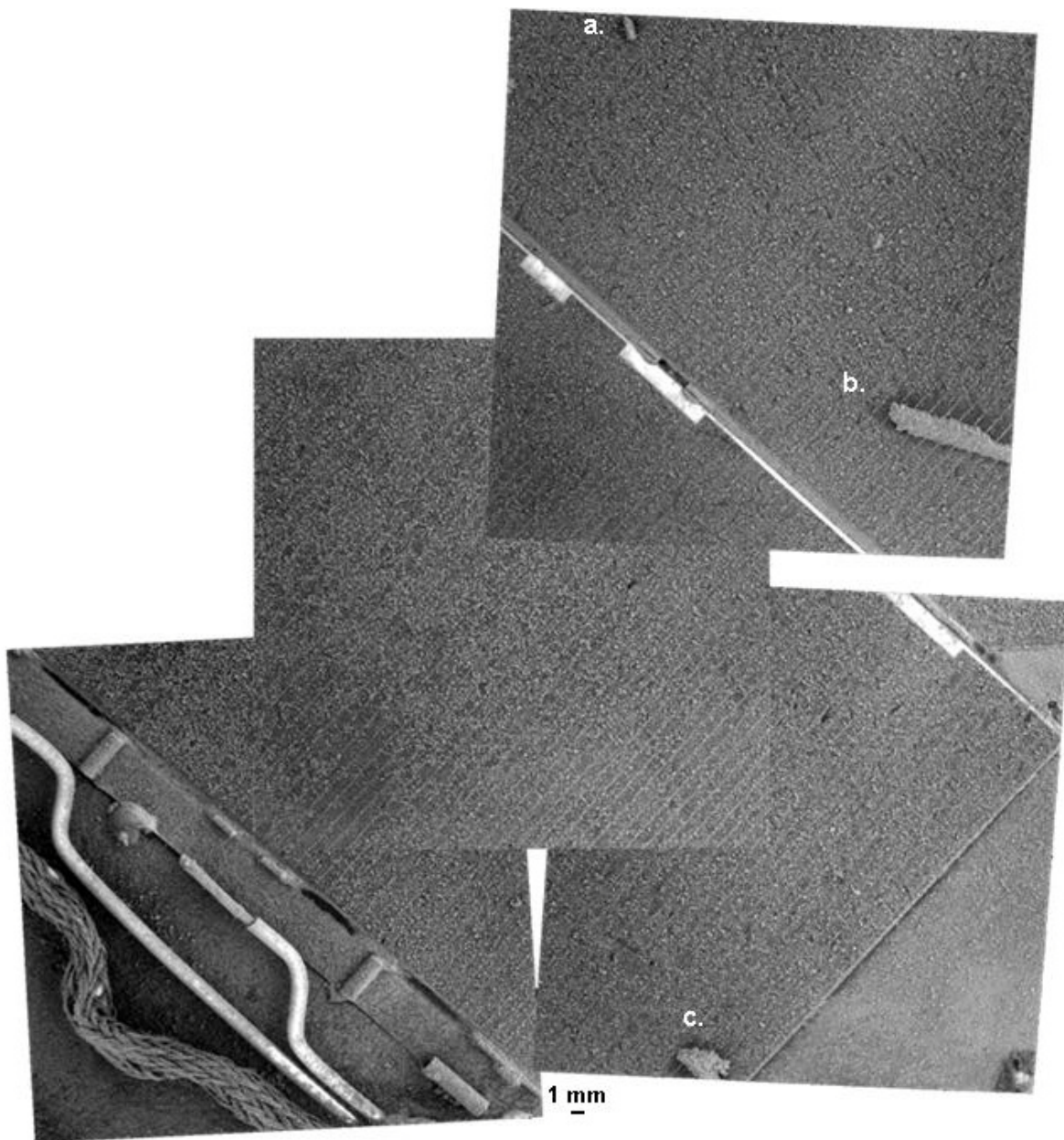


Figure 11. MI image mosaic of solar array from sol 1473. Note the 1 mm scale bar. Images were acquired in shadow. **(a)** The aggregate at the top of the mosaic is 1.5 mm long and 500 μm wide. **(b)** The elongated aggregate is >8 mm long by 1.5 mm wide. **(c)** The long axis is 3 mm long. ([figure11.jpg](#))

aggregates could be dust and/or soil deposits picked up from the surface by the Mössbauer or APXS and dropped onto the array when the robotic arm reached above the rover deck to take MI images. In this scenario, the larger soil/dust deposits from the arm would have had to incorporate the surrounding dust aggregates on the array during subsequent winds or vibration as a result of rover motion in order to produce the features seen in the MI images.

A single image was taken on sol 1506 (Figure 10e) of the adjacent section of the solar array showing the elongated aggregate. It had not changed appreciably since last seen on sol 1473.

Discussion

The “bright” capture magnet dust described in this work is spectrally consistent with bright soils and surface dust reported on elsewhere at the Gusev landing sight, as well as at the Opportunity, Pathfinder, and Phoenix landing sites (Bell et al. 2004; Yen et al. 2005; Bell et al. 2000; Leer et al. 2009). Spectra of these bright soils and surface dust are all characterized by steep visible slopes, 535 nm absorptions, reflectivity maximums between 700 and 1000 nm, and are relatively featureless in the NIR region. Previous work has shown these spectral characteristics to be consistent with nanophase ferric oxides rather than some other crystalline

iron oxide phase based on the lack of an electronic transition feature in the NIR ([Morris et al. 1990](#); [Morris et al. 1997](#)). This consistency among soils and dust measured from several locations on the surface further supports the theory that martian dust is globally mixed and deposited.

The spectral similarity between “dark” capture magnet dust and filter magnet dust, and their noted differences from the “bright” capture magnet dust suggest that they represent a lower albedo, more strongly magnetic component of the dust. [Kinch et al. \(2006\)](#) modeled such behavior of particles of different minerals according to their magnetic properties and [Madsen et al. \(2009\)](#) reported the dust to be magnetically separable in wind events, as can be seen by the population of much darker, and more strongly magnetic grains left on the capture magnet in the Sol 425 MI image, after the Sol 417 -420 cleaning event (Figure 8b). This pattern was observed again on the Sol 2017 capture magnet image (Figure 8f) following the latest cleaning event. The darker component of the dust must be more strongly magnetic, as it remains attached to the capture magnet in the presence of very strong winds that removed most of the “bright” dust, and adheres to the weaker filter magnet. The strongly magnetic component of the dust has been shown to be magnetite as revealed by Mössbauer data of dust on both the Spirit and Opportunity capture magnets ([Goetz et al. 2005](#); [Madsen et al. 2009](#)). Magnetite is also generally consistent with the characteristics of these dust spectra, which are that they are much less red than the bright dust, have lower overall reflectance values, and are featureless in the NIR region (Figure 6). However, if these particles were pure magnetite we would expect to see a negative NIR slope or a downturn towards an absorption feature around 1 μm . The absence of this downturn suggests that these particles are actually composites of magnetite and other minerals, which is also consistent with the Mössbauer data.

In addition to the dust aggregates observed on the rover magnets and solar array, this behavior has been seen in local surface deposits investigated by the Spirit rover, and was documented by [Sullivan et al. \(2008\)](#). Dust aggregates were also observed to form in suspension in wind tunnel experiments, some as large as 1-3 mm ([Merrison et al. 2004](#); [Merrison et al. 2007](#)). Martian dust grains tend to be triboelectrically charged ([Sickafoose et al. 2001](#)), and according to [Merrison et al. \(2004\)](#) the charging tends to occur upon dispersion of the dust into the wind tunnel. On Mars we might equate this with dust grains becoming electrically charged in a dust storm or any large wind event and forming aggregates in the air. There is no way to be certain whether the aggregates observed in this work were formed in situ or while airborne, although it is interesting that the MI images acquired around and after the 2007 dust storm (peaking around Sol 1250) show the most dust aggregates. However, the growth of aggregates between the Sol 1358 and 1473 filter magnet images, and the large aggregates imaged on the array on Sol 1473 suggest that dust aggregates can also form in situ.

The presence of sand grains on the magnets and the rover

body provides information on the depth of the saltation layer and wind speeds. The maximum heights of saltating particles on Mars are not well constrained as summarized by Greeley and Iversen (1985). We observe sand grains that have saltated to heights of at least 70 - 75 cm (rover deck and magnets, respectively) in strong wind events. However, the small amount of true sand grains identified on the rover body cannot imply much about the structure of the saltation layer since it is possible that these grains are high trajectory outliers. [Sullivan et al. \(2008\)](#) calculated the necessary friction speeds to move < 300 μm sand as seen on the rover body to be 1.7 to 2.1 m/s using the equations provided by Greeley and Iversen (1985), and equated that to wind speeds of 20 to 40 m/s at the height of the camera bar, 1.5 m.

Typical Viking I Lander wind speeds were between 5 and 10 m/s, however, wind speeds of 25-30 m/s were observed during dust storms and were associated with surface morphology changes in the form of eroding soil piles ([Arvidson et al. 1983](#)). During the Pathfinder Mission, no saltating grains or grains with appearances other than dust appeared on the magnets ([Madsen et al. 1999](#)) even at the lower heights of those magnets (25 and 50 cm above the surface). That is consistent with the low wind velocities measured throughout the mission of < 5 m/s ([Schofield et al. 1997](#)).

The Phoenix lander was equipped with a Telltale that allowed measurements of wind speeds and directions at a height of 2 m ([Gunnlaugsson et al. 2008](#)). Dust fibers were observed to collect on the Telltale and were removed only by very strong winds associated with dust devils on the order 35-40 m/s (Holstein-Rathlou et al. 2010; [Ellehoj et al. 2010](#)). The highest winds speeds outside of a dust devil were measured to be 16 m/s and the dust fibers were unaffected (Holstein-Rathlou et al. 2010). The Spirit rover is not equipped to directly measure wind speeds, but these measurements by other missions, in addition to the laboratory work of [Merrison et al. \(2002\)](#) and [Merrison et al. \(2007\)](#) allow for some constraints on wind speeds required for dust removal associated with the MER cleaning events. Consistent with these other measurements, it is reasonable to conclude that wind speeds in excess of 20 m/s at the height of the rover deck and magnets are capable of lifting large amounts of dust.

Wind tunnel experiments indicate that the particle size most easily set into motion by wind on Mars is 100-150 μm , while actual dust sized particles (< 4 μm diameter) should be more difficult to raise ([Greeley et al. 1980](#); [Iversen and White. 1982](#); Greeley et al. 1992). It has been shown that when saltating sand strikes the surface it kicks up dust grains that are then entrained by the wind ([White 1979](#); Greeley et al. 1992), implying that wind speeds sufficient to saltate sand are also responsible for contributing dust to the atmosphere. As suggested by [Merrison et al. \(2007\)](#) and [Sullivan et al. \(2008\)](#), dust aggregates observed to form in wind tunnel experiments and both in the local deposits and on the rover magnets and solar array that reach ~100 μm in diameter and larger should be easier to entrain due to their size and lower

density than individual dust grains or solid sand grains and could represent another process by which dust particle entrainment occurs. It should be noted that the details of this process are not well understood. [Bridges et al. \(2010\)](#) invoke saltating dust aggregates that compose bedforms and are later cemented to form a unit called dust-stone around the Tharsis volcanoes, and describe a process whereby dust aggregates form, get suspended, grow to a size where they are below the suspension threshold, saltate, and eventually grow too big to travel.

Summary

The Pancam and Microscopic Imager (MI) have been used to effectively monitor dust accumulation, removal, spectral characteristics, and morphology on the Spirit rover for over 2000 sols. Spirit has experienced three major cleaning events during which significant amounts of dust were removed from the vehicle. The effects of these events were observed with dust-monitoring Pancam images of the magnets and other rover hardware. These images also show the aggregating nature of dust particles on the rover deck.

Pancam multispectral data of dust deposits on the magnets can be divided into three different classes: "bright" capture magnet dust, "dark" capture magnet dust, and filter magnet dust. Bright capture magnet dust spectra have the highest reflectance levels, steep visible slopes (434 to 673 nm), and strong 535 nm absorptions. They have a convex shape and are relatively featureless in the NIR region (700 to 1000 nm). Bright capture magnet dust is consistent with dust and bright soils measured elsewhere on the martian surface and is likely composed of nanophase ferric oxides.

Dark capture magnet dust has the lowest reflectance levels of the three classes, and is much less "red" than the bright capture magnet dust. It has much shallower 535 nm absorptions than bright capture magnet dust, and is relatively featureless in the NIR region. It also exhibits positive slopes from 900 to 1000 nm. Filter magnet dust is spectrally similar to dark capture magnet dust as it is also much less "red" than the bright dust, has lower reflectance levels, shallower 535 nm absorptions, and the lack of any NIR features. These spectra represent a darker, more strongly magnetic component of the dust, which is believed to be at least partially composed of magnetite. Changes in lighting geometry over phase angles of 13-54° have been shown to have a minimal affect on the spectral characteristics described for dust on the magnets.

The MI shows various populations of grains on the rover ranging in size from dust (clumps composed of individual, unresolved grains) to fine sand (250 µm). MI images of the solar array reveal sand sized grains that have evidently saltated to a height of 70 cm in strong winds, helping to constrain saltation heights for the most easily saltated particles on Mars. Wind speeds in excess of 20 m/s at the height of the rover deck and magnets are responsible for the observed cleaning events involving the substantial removal of dust from the vehicle. MI views of both the magnets and

the solar array through sol 2017 illustrate that dust tends to aggregate to form larger particles up to mm(s) in size. These observations support the hypothesis that larger dust aggregates, which should be easier to entrain by wind than individual dust grains, are a significant contributor to atmospheric dust loading in addition to or in the absence of saltating sand.

Directory of supporting data

[root directory](#)

[vaughan mars 2010 0005.pdf](#)

Figure 1 [figure1a.jpg](#); [figure1b.jpg](#)

Figure 2 [figure2.jpg](#)

Figure 3 [figure3.jpg](#)

Figure 4 [figure4.jpg](#)

Figure 5 [figure5a.jpg](#); [figure5b.jpg](#); [figure5c.jpg](#); [figure5d.jpg](#); [figure5e.jpg](#); [figure5f.jpg](#); [figure5g.jpg](#); [figure5h.jpg](#)

Figure 6 [figure6.jpg](#); [figure6.txt](#)

Figure 7 [figure7a.jpg](#); [figure7b.jpg](#); [figure7c.txt](#); [figure7d.txt](#)

Figure 8 [figure8a.jpg](#); [figure8b.jpg](#); [figure8c.jpg](#); [figure8d.jpg](#); [figure8e.jpg](#); [figure8f.jpg](#); [figure8g.jpg](#)

Figure 9 [figure9a.jpg](#); [figure9b.jpg](#); [figure9c.jpg](#); [figure9d.jpg](#); [figure9e.jpg](#); [figure9f.jpg](#)

Figure 10 [figure10a.jpg](#); [figure10c.jpg](#); [figure10d.jpg](#); [figure10e.jpg](#)

Figure 11 [figure11.jpg](#)

Supplemental Figure 1 [suppfig1.pdf](#)

[suppfig1a.txt](#); [suppfig1b.txt](#); [suppfig1c.txt](#); [suppfig1d.txt](#); [suppfig1e.txt](#); [suppfig1f.txt](#); [suppfig1g.txt](#); [suppfig1h.txt](#)

Supplemental Figure 2 [suppfig2.pdf](#)

[suppfig2a.jpg](#); [suppfig2b.jpg](#); [suppfig2c.jpg](#); [suppfig2d.jpg](#); [suppfig2e.jpg](#); [suppfig2f.jpg](#); [suppfig2g.jpg](#); [suppfig2h.jpg](#); [suppfig2i.jpg](#); [suppfig2j.jpg](#)

Supplemental Figure 3 [suppfig3.pdf](#)

[suppfig3a.jpg](#); [suppfig3b.jpg](#); [suppfig3c.jpg](#); [suppfig3d.jpg](#); [suppfig3e.jpg](#); [suppfig3f.jpg](#); [suppfig3g.jpg](#); [suppfig3h.jpg](#); [suppfig3i.jpg](#); [suppfig3j.jpg](#)

Acknowledgements

We would like to thank Jennifer Herman, the MER power engineer, for helpful discussions regarding power values and acceptable presentation of the data, as well as the entire MER team for supporting the dust monitoring studies and acquiring the data. We would also like to thank our reviewers whose comments significantly improved the manuscript.

References

- Arvidson, R. E., E. A. Guinness, H. J. Moore, J. Tillman and S. D. Wall (1983) "Three Mars years - Viking Lander 1 imaging observations" *Science* 222, 463-468. [doi:10.1126/science.222.4623.463](#)
- Bell III, J. F. et al. (2000) "Mineralogic and compositional properties of Martian soil and dust: Results from Mars Pathfinder" *Journal of Geophysical Research* 105, 1721-1756. [doi:10.1029/1999JE001060](#)

- Bell III, J. F. et al. (2003) "Mars Exploration Rover Athena Panoramic Camera (Pancam) investigation" *Journal of Geophysical Research* 4, 8063. doi:[10.1029/2003JE002070](https://doi.org/10.1029/2003JE002070)
- Bell III, J. F. et al. (2004) "Pancam multispectral imaging results from the Spirit Rover at Gusev Crater" *Science* 305, 800-807. doi:[10.1126/science.1100175](https://doi.org/10.1126/science.1100175)
- Bell III, J. F., J. Joseph, J. N. Sohl-Dickstein, H. M. Arneson, M. J. Johnson, M. T. Lemmon and D. Savransky (2006) "In-flight calibration and performance of the Mars Exploration Rover Panoramic Camera (Pancam) instruments" *Journal of Geophysical Research* 111, E02S03. doi:[10.1029/2005JE002444](https://doi.org/10.1029/2005JE002444)
- Bertelsen, P. et al. (2004) "Magnetic properties experiments on the Mars Exploration Rover Spirit at Gusev Crater" *Science* 305, 827-829. doi:[10.1126/science.1100112](https://doi.org/10.1126/science.1100112)
- Bridges, N. T. et al. (2010) "Aeolian bedforms, yardangs, and indurated surfaces in the Tharsis Montes as seen by the HiRISE Camera: Evidence for dust aggregates" *Icarus* 205, 165-182. doi:[10.1016/j.icarus.2009.05.017](https://doi.org/10.1016/j.icarus.2009.05.017)
- Ellehoj, M. D. et al. (2010) "Convective vortices and dust devils at the Phoenix Mars mission landing site" *Journal of Geophysical Research* 115, E00E16. doi:[10.1029/2009JE003413](https://doi.org/10.1029/2009JE003413)
- Gellert, R. et al. (2004) "Chemistry of rocks and soils in Gusev Crater from the alpha particle X-ray spectrometer" *Science* 305, 829-833. doi:[10.1126/science.1099913](https://doi.org/10.1126/science.1099913)
- Goetz, W. et al. (2005) "Indication of drier periods on Mars from the chemistry and mineralogy of atmospheric dust" *Nature* 436, 62-65. doi:[10.1038/nature03807](https://doi.org/10.1038/nature03807)
- Greeley, R., R. Leach, B. White, J. Iversen and J. B. Pollack (1980) "Threshold windspeeds for sand on Mars - Wind tunnel simulations" *Geophysical Research Letters* 7, 121-124. doi:[10.1029/GL007i002p00121](https://doi.org/10.1029/GL007i002p00121)
- Greeley, R. and J. D. Iversen (1985) "Wind as a geological process on Earth, Mars, Venus and Titan" Cambridge Planetary Science Series (W. I. Axford, G. E. Hunt and R. Greeley editors) Cambridge University Press, Cambridge.
- Greeley, R., N. Lancaster, S. Lee and P. Thomas (1992) "Martian aeolian processes, sediments, and features" in Mars (H. H. Kieffer, B. M. Jakosky, C. W. Snyder and M. Matthews editors) 730-766, University of Arizona Press, Tucson.
- Greeley, R. et al. (2006) "Active dust devils in Gusev crater, Mars: Observations from the Mars Exploration Rover Spirit" *Journal of Geophysical Research* 111, E12S09. doi:[10.1029/2006JE002743](https://doi.org/10.1029/2006JE002743)
- Gunnlaugsson, H. P. et al. (2008) "Telltale wind indicator for the Mars Phoenix lander" *Journal of Geophysical Research* 113, E00A04. doi:[10.1029/2007JE003008](https://doi.org/10.1029/2007JE003008)
- Herkenhoff, K. E. et al. (2003) "Athena Microscopic Imager investigation" *Journal of Geophysical Research* 6, 8065. doi:[10.1029/2003JE002076](https://doi.org/10.1029/2003JE002076)
- Holstein-Rathlou, C., H. P. Gunnlaugsson, J. P. Merrison, P. Nørnberg, M. D. Ellehoj, K. M. Bean, M. T. Lemmon, L. Tamppari, P. Smith and the Phoenix Science Team (2010) "Time-dependent dust accumulation on the Mars Phoenix wind indicator" *Lunar and Planetary Science XXXI*, Abstract No. 1811, The Woodlands.
- Iversen, J. D. and B.R. White (1982) "Saltation threshold on Earth, Mars, and Venus" *Sedimentology* 29, 111-119. doi:[10.1111/j.1365-3091.1982.tb01713.x](https://doi.org/10.1111/j.1365-3091.1982.tb01713.x)
- Johnson, J. R. et al. (2006) "Spectrophotometric properties of materials observed by Pancam on the Mars Exploration Rovers: 1. Spirit" *Journal of Geophysical Research* 111, E02S14. doi:[10.1029/2005JE002494](https://doi.org/10.1029/2005JE002494)
- Kinch, K. M., J. P. Merrison, H. P. Gunnlaugsson, P. Bertelsen, M. B. Madsen and P. Nørnberg (2006) "Preliminary analysis of the MER magnetic properties experiment using a computational fluid dynamics model" *Planetary and Space Science*, 54, 28-44. doi:[10.1016/j.pss.2005.07.008](https://doi.org/10.1016/j.pss.2005.07.008)
- Landis, G. A. (2005) "Exploring Mars with solar powered rovers" Photovoltaic Specialists Conference. Conference Record of the 31st IEEE, 858-861. doi:[10.1109/PVSC.2005.1488268](https://doi.org/10.1109/PVSC.2005.1488268)
- Landis, G. A., K. Herkenhoff, R. Greeley, S. Thompson, P. Whelley and the MER Athena Science Team (2006) "Dust and sand deposition on the MER solar arrays as viewed by the microscopic imager" *Lunar and Planetary Science XXXVII*, Abstract No. 1932, League City.
- Leer, K., L. Drube, W. Goetz, P. Gunnlaugsson, M. Lemmon, M. B. Madsen, R. V. Morris, P. Smith and the Phoenix Science Team (2009) "Optical study of particles on Phoenix magnets" *Lunar and Planetary Science XL*, Abstract No. 1923, The Woodlands.
- Lemmon, M. T. et al. (2004) "Atmospheric imaging results from the Mars Exploration Rovers: Spirit and Opportunity" *Science* 306, 1753-1756. doi:[10.1126/science.1104474](https://doi.org/10.1126/science.1104474)
- Madsen, M. B., S. F. Hviid, H. P. Gunnlaugsson, J. M. Knudsen, W. Goetz, C. T. Pedersen, A. R. Dinesen, C. T. Mogensen, M. Olsen and R. B. Hargraves (1999) "The magnetic properties experiments on Mars Pathfinder" *Journal of Geophysical Research* 104, 8761-8780. doi:[10.1029/1998JE900006](https://doi.org/10.1029/1998JE900006)
- Madsen, M. B. et al. (2003) "Magnetic properties experiments on the Mars Exploration Rover mission" *Journal of Geophysical Research* 10, 8069. doi:[10.1029/2002JE002029](https://doi.org/10.1029/2002JE002029)
- Madsen, M. B. et al. (2009) "Overview of the magnetic properties experiments on the Mars Exploration Rovers" *Journal of Geophysical Research* 114, E06S90. doi:[10.1029/2008JE003098](https://doi.org/10.1029/2008JE003098)
- Merrison, J., H. Gunnlaugsson, L. Mossin, J. Nielsen, P. Nørnberg, K. Rasmussen and E. Uggerhøj (2002) "Capture of magnetic dust in a simulated Martian aerosol: the importance of aerodynamics" *Planetary and Space Science* 50, 371-374. doi:[10.1016/S0032-0633\(02\)00009-0](https://doi.org/10.1016/S0032-0633(02)00009-0)
- Merrison, J., J. Jensen, K. Kinch, R. Mugford and P. Nørnberg (2004) "The electrical properties of Mars analogue dust" *Planetary and Space Science* 52, 279-290. doi:[10.1016/j.pss.2003.11.003](https://doi.org/10.1016/j.pss.2003.11.003)
- Merrison, J. P., H. Gunnlaugsson, P. Nørnberg, A. E. Jensen and K. R. Rasmussen (2007) "Determination of the wind induced detachment threshold for granular material on Mars using wind tunnel simulations" *Icarus* 191, 568-580. doi:[10.1016/j.icarus.2007.04.035](https://doi.org/10.1016/j.icarus.2007.04.035) doi:[10.1016/j.pss.2003.11.003](https://doi.org/10.1016/j.pss.2003.11.003)
- Morris, R. V., J. L. Gooding, H. V. Lauer and R. B. Singer (1990) "Origins of Marslike spectral and magnetic properties of a Hawaiian palagonitic soil" *Journal of Geophysical Research* 95, 14427-14434. doi:[10.1029/JB095iB09p14427](https://doi.org/10.1029/JB095iB09p14427)
- Morris, R. V., D. C. Golden and J. F. Bell III (1997) "Low-temperature reflectivity spectra of red hematite and the color of Mars" *Journal of Geophysical Research* 102, 9125-9134. doi:[10.1029/96JE03993](https://doi.org/10.1029/96JE03993)
- Morris, R. V. et al. (2004) "Mineralogy at Gusev Crater from the Mössbauer Spectrometer on the Spirit Rover" *Science* 305, 833-837. doi:[10.1126/science.1100020](https://doi.org/10.1126/science.1100020)
- Reid, R. J. et al. (1999) "Imager for Mars Pathfinder (IMP) image calibration" *Journal of Geophysical Research* 104, 8907-8926. doi:[10.1029/1998JE900011](https://doi.org/10.1029/1998JE900011)
- Schofield, J. T., J. R. Barnes, D. Crisp, R. M. Haberle, S.

- Larsen, J. A. Magalhães, J. R. Murphy, A. Seiff and G. Wilson (1997) "The Mars Pathfinder atmospheric structure investigation/meteorology" *Science* 278, 1752. [doi:10.1126/science.278.5344.1752](https://doi.org/10.1126/science.278.5344.1752)
- Sickafoose, A. A., J. E. Colwell, M. Horányi and S. Robertson (2001) "Experimental investigations on photoelectric and triboelectric charging of dust" *Journal of Geophysical Research* 106, 8343-8356. [doi:10.1029/2000JA000364](https://doi.org/10.1029/2000JA000364)
- Sullivan, R. et al. (2008) "Wind-driven particle mobility on Mars: Insights from Mars Exploration Rover observations at "El Dorado" and surroundings at Gusev Crater" *Journal of Geophysical Research* 113, E06S07. [doi:10.1029/2008JE003101](https://doi.org/10.1029/2008JE003101)
- White, B. R. (1979) "Soil transport by winds on Mars" *Journal of Geophysical Research* 84, 4643-4651. [doi:10.1029/JB084iB09p04643](https://doi.org/10.1029/JB084iB09p04643)
- Yen, A. S. et al. (2005) "An integrated view of the chemistry and mineralogy of martian soils" *Nature* 436, 49-54. [doi:10.1038/nature03637](https://doi.org/10.1038/nature03637)